Three-axis optical force plate for studies in small animal locomotor mechanics

S. Tonia Hsieh
Department of Organismic and Evolutionary Biology, Harvard University, Cambridge, Massachusetts 02138

(Received 18 August 2005; accepted 27 March 2006; published online 26 May 2006)

The use of force plates to measure whole-body locomotor mechanics is a well-established technique. However, commercially available force plates are not sensitive enough for use on small-bodied vertebrates or invertebrates. The standard design for single- and multiple-axis, high-sensitivity force plates built by individual research groups uses semiconductor foil strain gauges to measure deflections; yet foil strain gauges are highly temperature and position sensitive, resulting in a drifting base line and nonlinear responses. I present here a design for a three-axis optical force plate that was successfully calibrated to measure forces as small as 1.5 mN and is capable of determining the position of center of pressure with a mean error of 0.07 cm along the *X* axis and 0.13 cm along the *Y* axis. Using optical sensors instead of foil strain gauges to measure deflection, this force plate is not subject to temperature-related drift and is more robust against slight positioning inaccuracies. This force plate was used to measure forces produced by amphibious fishes weighing less than 2 g as they jumped off the force platform. © *2006 American Institute of Physics.*
[DOI: 10.1063/1.2202910]

I. BACKGROUND

How animals move and maintain stability during locomotion is of major interest to biomechanics and robotics researchers.[1–12] The use of force plates to study terrestrial locomotor mechanics is a well-established technique.[11,12] As an animal runs across a force platform mounted flush to a locomotor surface, the platform returns measurements of the magnitude of surface reaction forces. By recording these reaction forces and combining these data with position and velocity information extracted from video footage, it is possible to calculate torques and other forces acting about joints or the center of mass, both of which have important implications for the whole-body mechanics of locomotion.

One of the most dramatic examples of efficient high-speed locomotion by an inherently unstable locomotor system is demonstrated by a small-bodied, amphibious fish, the Pacific leaping blenny (*Alticus arnoldorum*). These blennies are found out of water along wave-swept intertidal zones in the tropical Pacific and have a remarkably diverse locomotor repertoire[13] which permits them to navigate in such a harsh environment. Despite their unusually terrestrial habits, these blennies have no obvious morphological adaptations which would permit them to move about on land more effectively than any other fully aquatic fish. As a result, it was of interest to examine the terrestrial locomotor mechanics of these blennies to discover how they are able to use fins adapted for aquatic locomotion on land.

The conceptual design of a force plate is simple and usually consists of a platform attached to a beam, or series of beams, which deforms in a known location. Beam configuration varies depending on whether the plate needs to measure one, two, or all three axes of force. To limit beam deformation to a known location, material on the beam is removed to create a blade, around which the beam bends, such that the blade and beam are made of the same piece of material. When a force is exerted against the platform, there is a measurable deformation of the blade which falls within the linear response range of its material. The amount of blade displacement is then calibrated against a range of known masses to determine the magnitude of force.

Important considerations in the design of a force plate include ensuring that the force plate's resonant frequency is significantly greater than the frequencies from the measured signal, permitting selection of a cut-off frequency that will minimally attenuate the actual signal—usually set at ten times the frequency of a locomotor event—and selecting a stiff but light enough material for the platform such that the platform itself does not deform when loaded with the maximum expected force. Also, if the plate is to measure more than one axis of force, cross talk between the axes is kept to a minimum.[12]

Most commercial force plates (e.g., from Kistler Instrument Corp. or Advanced Mechanical Technology, Inc.) are built for studies of human gait and are therefore inappropriate for smaller animal studies. The Pacific leaping blenny weighs less than 2 g, requiring a force plate that can measure forces in the millinewton range. Force plates that can be used for animals of this mass are very expensive to commission and equally difficult to build on one's own. The standard design for force plates used for small-bodied vertebrates and invertebrates uses semiconductor foil strain gauges to measure deflection.[12] To amplify the signal from blade deflection, these strain gauges are mounted in pairs on beams—one measuring compression and the other tension. Two pairs of strain gauges for each axis in the front and rear of the force plate are then configured to form a Wheatstone bridge. Although semiconductor strain gauges have the advantage of

being easy to attach to the blades—they are simply glued in place with Epoxy—they must be positioned very accurately on the blades to ensure a linear response. Additionally, they are extremely temperature sensitive and will continually drift during each experimental session as a result of temperature changes due to current flow when the equipment is powered on and heat from bright illumination required for high-speed video taping.[14]

I present here the design of a triaxial force plate that uses optical sensors as strain gauges, thereby circumventing the difficulties associated with temperature changes and foil strain gauge positioning problems. This force plate permits measurement of force along three axes simultaneously as well as determination of center of pressure position on the platform surface. Additionally, the design is unique in that it permits sensitivity adjustments by switching out the blades according to the requirements of the system to be studied. This force plate was used to quantify the land-based jumping forces produced by Pacific leaping blennies to understand how these blennies maintain locomotor stability on land.

II. MATERIALS AND METHODS

A. Optical sensor and LED

Photodetectors (SPOT-2DMI) were purchased from UDT Sensors, Inc. (Hawthorne, CA). These photodetectors are segmented into two active areas separated by a 0.13 mm element gap. Spectral response range is 350–1100 nm with peak responsivity between 900 and 1000 nm. These sensors are designed to have position resolutions of better than 0.1 μm and are stable over time and temperature. Amplification circuits were modified after the typical biasing and detection circuitry provided by UDT Sensors Inc.

High-intensity red light-emitting diodes (LEDs) were purchased from SunLED (Walnut, CA). Although the peak emission wavelengths of these LEDs are slightly lower than the peak responsivity range of the photodetectors, using a LED that emitted within the visible light spectrum allowed visual confirmation that the light spot was centered over the photodetector active area.

B. Force plate design

The triaxial force plate design [Figs. 1(a) and 1(b)] is based on one commonly used for semiconductor strain gauge force plates.[15] The platform was made of balsa wood and supported on two ends by beams made of square, hollow brass. Each of the beams had six sets of brass blades—three sets at each corner—positioned such that they each bent only in the X (fore-aft), Y (left-right), or Z (vertical) direction. The blades were paired and fixed to opposite sides of the beam such that the moment of mass was distributed away from the neutral axis, effectively stiffening the bending point and minimizing cross talk between channels. To determine the thickness of paired blades required to reflect the desired sensitivity, the equivalent double-blade thickness was calculated using beam theory[16] and can be derived as follows:

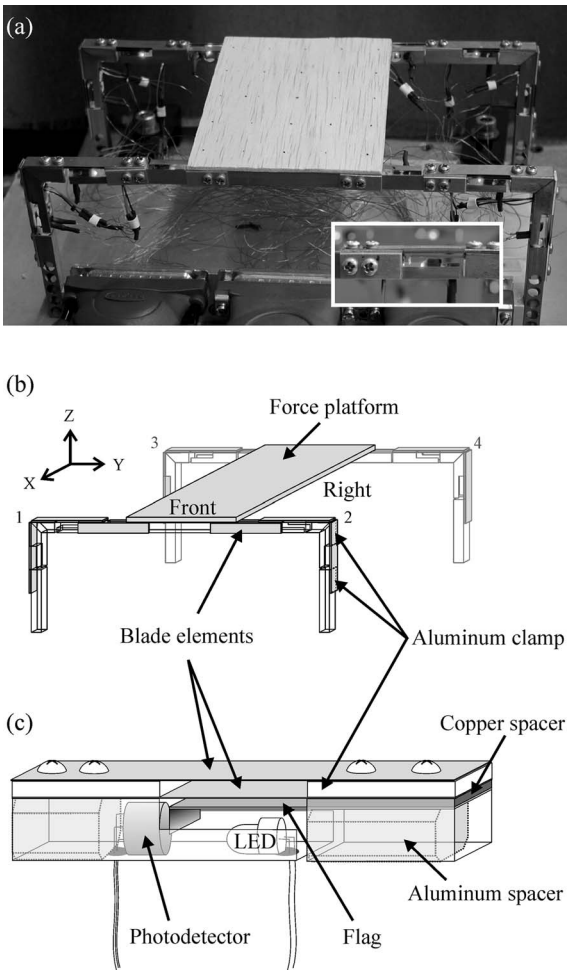

FIG. 1. (a) Schematics of the force plate and (b) an enlarged view of the photodetector setup. Twelve total photodetector setups were present on the force plate with three at each corner of the force plate for the X, Y, and Z axes.

$$F = \frac{12EI\Delta}{L^3}, \tag{1}$$

for which F is the force required to deflect a blade of length L a distance Δ. E is the material's Young's modulus and I is the moment of inertia defined as

$$I = \frac{1}{12}WH^3. \tag{2}$$

W is the width of the blade and H the thickness. Equation (1) applies only to the bending of a single beam, so it needs to be generalized to two beams to be relevant to the force plate design. If the two beams are of identical material but of different thicknesses (H_1 and H_2), then the total force F_{new} to displace the two beams a new distance Δ_{new} would be

$$F_{\text{new}} = F_1 + F_2 = \frac{12EI_1\Delta_{\text{new}}}{L^3} + \frac{12EI_2\Delta_{\text{new}}}{L^3} = \frac{EW\Delta_{\text{new}}}{L^3}(H_1^3 + H_2^3), \tag{3}$$

for which F_1, F_2, I_1, and I_2 are the deflection forces and

moments of inertia for blades 1 and 2, respectively. Since the single beam and the double beam configuration should have the same stiffness ($F_{old}=F_{new}$) and thus identical deflections ($\Delta_{old}=\Delta_{new}$) per unit force,

$$F_{old}=\frac{EW\Delta_{old}H_{old}^3}{L^3}=\frac{EW\Delta_{new}}{L^3}(H_1^3+H_2^3), \tag{4}$$

$$H_{old}=\sqrt[3]{H_1^3+H_2^3}, \tag{5}$$

for which H_{old} is the thickness of the single blade and H_1 and H_2 are the thicknesses of each of the new blades. The force plate sensitivity could be adjusted by using combinations of blades of various thicknesses and bolting them to the beams accordingly. For the purposes of this experiment, blades 0.013 and 0.018 cm thick were used.

Each of the blade pairs were outfitted with a sensor setup [Fig. 1(a) inset and Fig. 1(c)], totaling twelve channels—four channels per axis—for the full force plate. The optical sensor and LED were mounted in the hollow core of the beam with a flag, a thin piece of aluminum bent at a right angle, intercepting the light beam such that it casts a shadow on the optical sensor. Movement of the shadow across the active areas of the photodetector enabled measurement of blade displacement.

C. Force plate calibration procedure

Force plate calibration consisted of a signal-force and a signal-position calibration. The signal-force calibration correlated the force plate's individual channel responses with the load force applied to the platform. These data were then used to complete the signal-position calibration which enabled localization of the center of pressure as applied to the force platform surface. For both calibration procedures, known loads were limited to being applied along one axis. In this article, the axis being calibrated will be referred to as the primary axis or the primary load axis. The other two axes will be referred to as secondary axes or secondary load axes.

Prior to starting calibration procedures, all channels were zeroed with the force plate unloaded. Gains were adjusted to be the same between the channels by placing a known mass on the plate and confirming that the signal output was identical among all channels for each axis.

1. Signal-force calibration protocol

When a load is applied along the primary axis, low-level responses will also be measured along the secondary axes. Since this cross talk between axes is inevitable, the actual load force is equal to the sum total of the signal response of the primary axis ($s_{1\cdots4}$) under load and a correction factor representing the cross talk signal response of the other axes ($s_{5\cdots12}$):

$$F_L=mg=a_1s_1+a_2s_2+a_3s_3+a_4s_4+a_5s_5+a_6s_6+a_7s_7+a_8s_8+a_9s_9+a_{10}s_{10}+a_{11}s_{11}+a_{12}s_{12}+a_{13}, \tag{6}$$

for which $a_{1\cdots13}$ are constants of the signal-force calibration.

Known calibration masses ($m=158$ mg to 14.4 g) were placed in the middle of the force platform to calibrate the four Z channels. The horizontal axis (X and Y) channels were calibrated by hanging masses off a thin tape that was attached to the force plate via a pin, then draped over an air pulley [Fig. 2(a)]. When k weights were used for the calibration, Eq. (6) can be written in matrix form as

$$\begin{bmatrix} F_L^{(1)} \\ F_L^{(2)} \\ \vdots \\ F_L^{(k)} \end{bmatrix} = \begin{bmatrix} s_1^{(1)} & s_2^{(1)} & s_3^{(1)} & s_4^{(1)} & s_5^{(1)} & s_6^{(1)} & s_7^{(1)} & s_8^{(1)} & s_9^{(1)} & s_{10}^{(1)} & s_{11}^{(1)} & s_{12}^{(1)} & 1 \\ s_1^{(2)} & s_2^{(2)} & s_3^{(2)} & s_4^{(2)} & s_5^{(2)} & s_6^{(2)} & s_7^{(2)} & s_8^{(2)} & s_9^{(2)} & s_{10}^{(2)} & s_{11}^{(2)} & s_{12}^{(2)} & 1 \\ \vdots & \vdots & \vdots & \vdots & \vdots & \vdots & \vdots & \vdots & \vdots & \vdots & \vdots & \vdots & \vdots \\ s_1^{(k)} & s_2^{(k)} & s_3^{(k)} & s_4^{(k)} & s_5^{(k)} & s_6^{(k)} & s_7^{(k)} & s_8^{(k)} & s_9^{(k)} & s_{10}^{(k)} & s_{11}^{(k)} & s_{12}^{(k)} & 1 \end{bmatrix} \begin{bmatrix} a_1 \\ a_2 \\ a_3 \\ a_4 \\ a_5 \\ a_6 \\ a_7 \\ a_8 \\ a_9 \\ a_{10} \\ a_{11} \\ a_{12} \\ a_{13} \end{bmatrix}, \tag{7}$$

and solved using a least squares fit for the a constant vector. Since the signals were zeroed prior to calibration, a_{13} is approximately zero and a_is_i ($i=1\cdots4$) represent the force F_i measured by each of the four channels per axis. This becomes important for the signal-position calibration method discussed next.

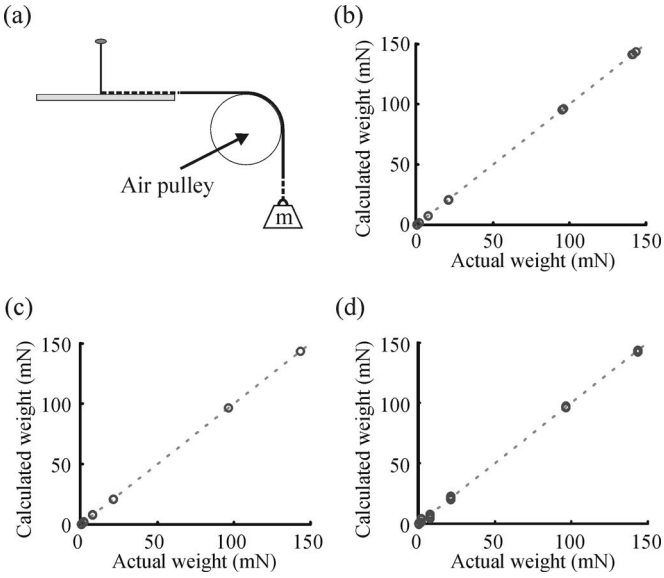

FIG. 2. Signal-force calibration results. (a) Schematic of the calibration setup. The thick, solid line is the tape and the dotted lines are string. The calibration mass is labeled as *m*. Individual channel calibration results were plotted against the actual calibration weight for the (b) *X* axis, (c) *Y* axis, and (d) *Z* axis. The dotted lines are the linear regressions. Slopes for all axes were 1.00, with $R^2 > 0.999$.

2. Signal-position calibration protocol

Equidistant points were marked off in a grid on the force platform and a single known mass was placed at each point to obtain *Z*-axis channel responses. Since the total torque (τ_{total}) acting on any static object is always zero, position calibration curves were derived by calculating the torques acting on each channel ($\tau_{1\ldots4}$) for the *Z* axis,

$$\tau_{\text{mass}} = \tau_1 + \tau_2 + \tau_3 + \tau_4 = 0,$$

$$F_L X = b_1 F_1 + b_2 F_2 + b_3 F_3 + b_4 F_4,$$

$$F_L Y = b_5 F_1 + b_6 F_2 + b_7 F_3 + b_8 F_4, \tag{8}$$

and solving for *X* and *Y* which are the positions on the force platform at which the mass is placed. Since cross talk between axes was low (see Sec. III), the uncorrected force value for each channel, $a_i s_i$, was used as the value for F_i. The constants $b_{1\ldots8}$ are the perpendicular distances of the *Z*-axis sensors from the platform origin. If the weight is placed at *p* positions, the following system of matrices represents the calibration scheme and it is possible to solve for the vector of *b* constants using a least squares fit:

$$\begin{bmatrix} X^{(1)} \\ Y^{(1)} \\ X^{(2)} \\ Y^{(2)} \\ \vdots \\ X^{(p)} \\ Y^{(p)} \end{bmatrix} = \begin{bmatrix} F_1^{(1)}/F_L^{(1)} & F_2^{(1)}/F_L^{(1)} & F_3^{(1)}/F_L^{(1)} & F_4^{(1)}/F_L^{(1)} & 0 & 0 & 0 & 0 \\ 0 & 0 & 0 & 0 & F_1^{(1)}/F_L^{(1)} & F_2^{(1)}/F_L^{(1)} & F_3^{(1)}/F_L^{(1)} & F_4^{(1)}/F_L^{(1)} \\ F_1^{(2)}/F_L^{(2)} & F_2^{(2)}/F_L^{(2)} & F_3^{(2)}/F_L^{(2)} & F_4^{(2)}/F_L^{(2)} & 0 & 0 & 0 & 0 \\ 0 & 0 & 0 & 0 & F_1^{(2)}/F_L^{(2)} & F_2^{(2)}/F_L^{(2)} & F_3^{(2)}/F_L^{(2)} & F_4^{(2)}/F_L^{(2)} \\ \vdots & \vdots & \vdots & \vdots & \vdots & \vdots & \vdots & \vdots \\ F_1^{(p)}/F_L^{(p)} & F_2^{(p)}/F_L^{(p)} & F_3^{(p)}/F_L^{(p)} & F_4^{(p)}/F_L^{(p)} & 0 & 0 & 0 & 0 \\ 0 & 0 & 0 & 0 & F_1^{(p)}/F_L^{(p)} & F_2^{(p)}/F_L^{(p)} & F_3^{(p)}/F_L^{(p)} & F_4^{(p)}/F_L^{(p)} \end{bmatrix} \begin{bmatrix} b_1 \\ b_2 \\ b_3 \\ b_4 \\ b_5 \\ b_6 \\ b_7 \\ b_8 \end{bmatrix}. \tag{9}$$

D. Data collection

Fishes were induced to jump off the force plate in the *X* direction. Each jump was recorded with one high-resolution (1024×1024), high-speed camera (Photron Ultima APX, San Diego, CA) filming at 500 frames/s, zoomed in on the lateral view of the force platform and fish, and one camcorder (Sony Handycam model DCR-TRV38) simultaneously filming the lateral and dorsal (via a 45° mirror) views of the entire length of the jump. A 0.5 cm grid was positioned in the background to permit video calibration and extraction of jump distance and height. The analog force plate response signals were electronically amplified, then converted to a digital signal using an ADInstruments (Colorado Springs, CO) analog-digital converter. Data were sampled at 1–10 kHz and recorded on a laptop computer with POWERLAB CHART5.0 (ADInstruments, Colorado Springs, CO) software. Jump force during a trial was calculated using the *a* vector of constants determined during the signal-force calibration.

E. Confirming force plate accuracy

The blenny was modeled as a point-mass projectile initially subject to three forces in the *X*, *Y*, and *Z* directions. Time to peak height t_p, maximum jump height $z(t_p)$, and jump distance d_{jump} were determined to be

$$t_p = \dot{z}(0)/g, \tag{10}$$

$$z(t_p) = \dot{z}^2(0) t_p / 2g, \text{ and} \tag{11}$$

$$d_{\text{jump}} = 2 t_p \sqrt{\dot{x}^2(0) + \dot{y}^2(0)}. \tag{12}$$

Calculated values for jump height and distance were then compared with those determined from the video images. The moment when the blenny's tail left the locomotor surface was set as $t=0$.

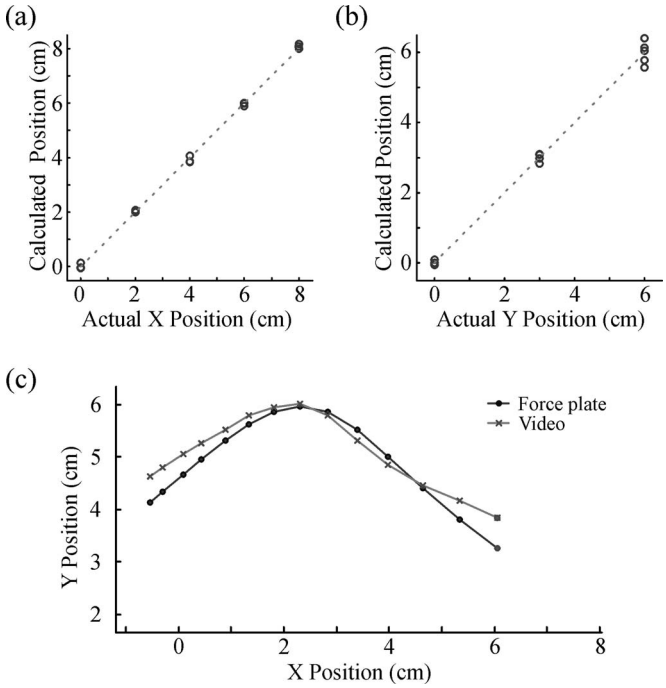

FIG. 3. Signal-position calibration results for real vs. calculated (a) X position and (b) Y position. In both panels, the fitted linear regression (dotted lines) have a slope of 1.00, $R^2=0.999(X)$ and $0.995(Y)$, and $p<0.001$. (c) Ball-rolling experiment result. X-Y position plots of ($\times$) the ball position digitized from video footage and (●) the ball position calculated from individual force plate Z-axis channel output.

To assess accuracy of center of pressure determination, a 1.06 g steel ball bearing was rolled across the force platform and filmed in dorsal view. The motion of the steel ball was then digitized and the calculated position data were then compared with the actual, digitized data for confirmation of center of pressure accuracy.

III. RESULTS AND DISCUSSION

A. Force plate calibration results

Force calibration and position calibration curves were linear, all with $R^2>0.995$ [Figs. 2(b)–2(d), 3(a), and 3(b)]. Force plate natural frequency was much lower than desired (31.1–46.5 Hz) because the moving elements of the force plate were heavy relative to the blades' spring stiffness. Mean cross talk between channels were 4.3% from X to Y, 0.6% from X to Z, 0.6% from Y to X, 8.2% from Y to Z, 8.1% from Z to X, and 4.4% from Z to Y.

B. Experimental results

When rolling a ball across the surface of the force plate, calculation of the location of center of pressure matched up well [Fig. 3(c)], with maximum errors of 0.56 and 0.41 cm at the start and end of the roll when the ball was moving most rapidly. Mean errors were 0.07 cm along the X axis and 0.13 cm along the Y axis. The apparent mismatch between calibration accuracy along the Y axis as shown in Fig. 3(b) with the calculated results in panel (c) may be caused by two factors. First, the system was not fully modeled and therefore some characteristics of force plate response, such as damping elements, were not accounted for. A more rigorous model of the dynamic components of the system would increase its positional accuracy. Second, the positional calibration as described here assumes the cross talk between channels is negligible when determining the center of pressure location. Although cross talk was shown to be less than 10% among all axes, this assumption likely introduced some error into the final center of pressure localization calculations.

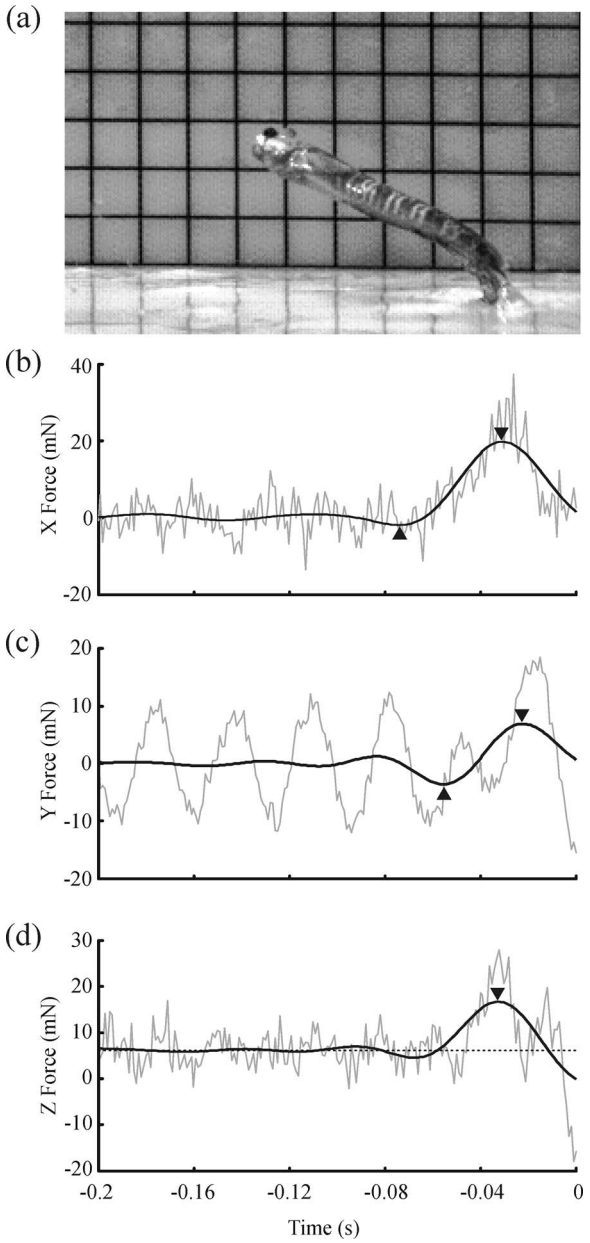

FIG. 4. Jumping blenny data. (a) A single high-speed video frame of a Pacific leaping blenny jumping off a horizontal surface on land. Representative unfiltered (gray line) and filtered (black line) force traces of a 0.6 g blenny jumping off the force plate for the (b) X axis, (c) Y axis, and (d) Z axis. The black triangles represent the location of peak (▼) positive and (▲) negative forces used to calculate signal/noise ratios presented in Table I. The dotted line in panel (d) is the fish's body weight (in mN). The blenny's tail loses contact with the surface at $t=0$ s.

The forces generated along each axis during an actual blenny jump are shown in Fig. 4. All data were filtered with a ninth-order Butterworth low-pass filter with a cut-off frequency of 20 Hz. A high order for the filter was chosen to increase the steepness of signal drop-off. For the trial shown

TABLE I. Signal-noise (SNR) for each axis.

	Positive		Negative	
Axis	Signal (mN)	SNR	Signal (mN)	SNR
X	19.71	4.36	−1.86	0.41
Y	6.86	1.05	−3.55	0.54
Z	16.68	4.46	···	···

in Fig. 4, forces along the *X* and *Y* axes had significant positive and negative components, whereas the *Z* axis only had a significant positive component. Signal to noise ratios (Table I) were calculated as the ratio of peak signal root mean square (rms) values with base line noise rms. The rms for the signal was calculated over 5 ms centered on the signal positive or negative peak. The rms for the noise was calculated over 80 ms of base line data. Over five jumps, calculated jump height and distance were within 0.6 and 0.9 cm of those values extracted from video sequences, respectively.

C. Force plate design considerations

Although this force plate worked well for the intended study, the current design may not be appropriate for all small animal locomotion experiments. Factors to consider prior to building this force plate include its low natural frequency and low signal to noise ratio, especially along the *Y* axis. It is also necessary to confirm that the plate is responding within the linear region of the sensors.

Decreasing the weight of the beams would substantially increase the plate's natural frequency because natural frequency is inversely related to the square root of the effective mass of the moving parts of the system. Two sources of "extra" weight in this system are the beam material and the beam design. The force plate beams described here are constructed of brass, which is three times heavier than aluminum. Since the absolute peak forces exerted upon the system are low, aluminum is sufficiently stiff for this application, and would serve to nearly double the natural frequency of the force plate. One of the primary considerations when building this force plate was to minimize material and construction costs. Brass was chosen as beam material for this force plate because extruded, hollow, square beams are more readily available than those made of aluminum, and therefore relatively inexpensive. The beams were designed so that the blade elements could be exchanged and thus the force plate sensitivity adjusted according to study requirements. However, the extra aluminum clamps, spacers, and bolts [Figs. 1(b) and 1(c)] added substantial mass to the system. If the blade elements are machined out of a single piece of metal, this could also serve to lower the mass of the moving elements on the beams, increasing the force plate's natural frequency.

Sensor response linearity is largely dependent on how evenly the light spot is distributed across the active sensor region. Tests on the sensors mounted in the force plate beams showed the electrical response of the sensor rapidly reached a plateau at a maximum or minimum voltage outside the linear region. The flag was therefore positioned such that the voltage output did not plateau at its most extreme displacement, determined by loading the platform with the maximum expected weight. While this positioning method increased the chance that the flag displaced only within the detector's linear response region, it did not ensure this.

The low signal to noise ratio may have resulted from the photodiode, external light sources, or force plate geometry. UDT Sensors, Inc., the manufacturer of the photodiodes, identifies two sources of noise in a photodiode: Johnson and shot noise. These sources of noise cannot be eliminated because they are associated with the material properties of the photodiode. Noise associated with external light sources can be reduced by shading the beams from the high-wattage lights required for high-speed video filming. In the study conducted here, however, the external light sources did not appear to contribute to the signal noise, and only acted to shift the signal base line when they were turned on or off.

A final method to decrease the noise to signal ratio would be to increase the signal magnitude rather than decrease the noise. It is likely that some of the difficulties associated with high noise resulted from the majority of peak horizontal forces being less than 30 mN (approximately 0.2–0.5 V response). Decreasing the spring constants of the horizontal axis blade elements or decreasing the distance between the flag and the LED would increase flag displacement and thus increase the signal response without further increasing the base level noise.

The force plate design and calibration protocols described here permit the collection of informative and useful locomotor force data in the range of 2–150 mN of force when the locomotor bout consists of an isolated movement. Total cost of construction (i.e., materials and commissioned labor for machining the beams) is substantially less than that required to build a semiconductor strain gauge force plate, largely because machining the individual parts is less labor intensive. A force plate using optical sensors as strain gauges has the added advantage of being temperature insensitive in comparison to semiconductor strain gauges. It is important to note, however, that constraints in the design and performance of this platform make the current design somewhat less appropriate for studies in which multiple cyclical locomotor bouts must be quantified.

ACKNOWLEDGMENTS

Many thanks to the following people for discussions about the force plate and amplifier circuitry designs and calibration procedures, as well as comments on versions of the article: Erik Anderson, Ben Arlett, Jacquie Ashmore, Eric Dufresne, Mark Finlayson, George Lauder, Jim MacArthur, Peter Madden, Eric Tytell, and Bill Walker. The initial idea was conceived in discussions with Michael Dickinson, Wyatt Korff, and Adam Summers. This project was funded by the National Geographic Society Research and Exploration Grant, the National Science Foundation Pre-doctoral Fellowship, the Harvard University Department of Organismic and Evolutionary Biology Graduate Dissertation Fund, and the Museum of Comparative Zoology Putnam Grant.

[1] I. K. Bartol, G. Morteza, D. Weihs, P. W. Webb, J. R. Hove, and M. S. Gordon, J. Exp. Biol. **206**, 725 (2003).
[2] E. G. Drucker and G. V. Lauder, J. Exp. Biol. **203**, 2279 (2000).
[3] F. E. Fish, J. Hurley, and D. P. Costa, J. Exp. Biol. **206**, 667 (2003).
[4] J. E. Harris, J. Exp. Biol. **13**, 476 (1936).
[5] Y.-C. Pai and K. Iqbal, J. Biomech. **32**, 779 (1999).
[6] M. G. McCay, J. Exp. Biol. **204**, 2817 (2001).
[7] D. L. Jindrich and R. J. Full, J. Exp. Biol. **205**, 2803 (2002).
[8] J. Schmitt, M. Garcia, R. C. Razo, P. Holmes, and R. J. Full, Biol. Cybern. **86**, 343 (2002).
[9] M. Sun and Y. Xiong, J. Exp. Biol. **208**, 447 (2005).
[10] L. H. Ting, R. Blickhan, and R. J. Full, J. Exp. Biol. **197**, 251 (1994).
[11] G. A. Cavagna, J. Appl. Physiol. **39**, 174 (1985).
[12] A. A. Biewener and R. J. Full, in *Biomechanics—Structures and Systems: A Practical Approach*, edited by A. A. Biewener (Oxford University Press, Oxford, 1992), pp. 45–73.
[13] M. Bhikajee and J. M. Green, African Zoology **37**, 221 (2002).
[14] R. Blickhan and R. J. Full, in *Biomechanics—Structures and Systems: A Practical Approach*, edited by A. A. Biewener (Oxford University Press, Oxford, 1992), pp. 75–96.
[15] N. C. Heglund, J. Exp. Biol. **93**, 333 (1981).
[16] F. P. Beer and E. R. Johnston, Jr., *Mechanics of Materials* (McGraw-Hill, New York, 1992), p. 740.